Chemical Physics Letters 550 (2012) 15–18

Contents lists available at SciVerse ScienceDirect

Chemical Physics Letters

journal homepage: www.elsevier.com/locate/cplett

Photoelectron spectroscopy and photochemistry of tetracyanoethylene radical anion in the gas phase

Dmitry Khuseynov, Matthew T. Fontana [1], Andrei Sanov *

Department of Chemistry and Biochemistry, The University of Arizona, Tucson, AZ 85721, USA

ARTICLE INFO

Article history:
Received 31 July 2012
In final form 18 August 2012
Available online 4 September 2012

ABSTRACT

A combined photoelectron spectroscopy, photofragmentation and clustering study of the tetracyanoethylene (TCNE) radical anion in the gas phase is reported. The adiabatic electron affinity of TCNE is 3.16(2) eV. This result represents an order-of-magnitude improvement in the uncertainty over the presently accepted, indirectly determined value. The photodissociation of the anion at 355 and 266 nm leads to three anionic channels: one yielding CN^- and the other two corresponding to the loss of one or two CN groups from the parent anion. The CN^- fragment channel is dominant at 355 nm, while the double-dissociation channel dominates 266 nm photochemistry.

1. Introduction

In the past decades, a considerable effort has been devoted to the preparation and study of molecule-based conductors, superconductors, and magnets. Electron-donor and electron-acceptor molecules play a major role in their development. One type of these molecules is organocyanides, which have been used extensively in materials chemistry due to their electron-acceptor properties and ability to form stable charge-transfer complexes and salts [1]. Thorough characterization of these molecules, especially their electron acceptance properties, is essential for understanding the bulk properties of the materials that contain them, as well as for the design of novel materials with enhanced characteristics.

Tetracyanoethylene (TCNE), the forerunner molecule in the class of strong electron acceptors [2], is well known for its highly conjugated π-system, which accounts for its unique reactivity [3]. The D_{2h} symmetry equilibrium structure of TCNE [4,5] is shown schematically in the inset in Figure 1. This molecule is an exceptionally strong dienophile [6]. It plays an integral role in many substitution and addition reactions, such as the Diels–Alder reactions [2], and is used as an oxidizing agent in the preparation of organic magnets, conductors [7], and superconductors [8]. It is also known to form stable charge-transfer complexes with many organometallic substrates, which makes it a key component for study of electron-transfer reactions [9].

Despite the variety of applications in materials and organic chemistry [6], some key properties of TCNE and the corresponding reduced anion are still in question. For example, the adiabatic electron affinity (EA) of TCNE has been evaluated only indirectly through gas-phase electron-transfer equilibrium and the presently accepted value EA = 3.17 ± 0.20 eV [10] encompasses a broad uncertainty range. The molecular structure and stability of neutral and reduced TCNE have been studied theoretically [4,5], but the results vary significantly depending on the level of theory. For example, the MP2/aug-cc-pVDZ calculations predict EA = 2.17 eV, while CCSD/aug-cc-pVDZ (at the B3LYP/aug-cc-pVDZ optimized geometries of the anion and the neutral) yields EA = 3.00 eV [4].

In the present work, we generate the $TCNE^-$ radical anion in the gas phase and examine its photodetachment and photochemistry using photoelectron imaging and photofragment mass-spectroscopy. We report the first direct spectroscopic determination of the electron affinity of TCNE, significantly improving on the uncertainty of the previous result. We also examine the anion clustered with water or argon and report the solvation effects on the anion stability. These clustering studies shed additional light on the delocalized charge distribution in the anion of TCNE.

2. Experimental section

The experiments were performed using a tandem time-of-flight reflectron mass-spectrometer described in detail previously [11]. A sample holder with TCNE powder was heated to 150 °C in order to increase the vapor pressure. The resulting TCNE vapor seeded in an Ar carrier gas with a backing pressure of 20 psi was introduced into a high-vacuum chamber through a pulsed nozzle (General Valve, Series 9) operated at a repetition rate of 50 Hz. The supersonic expansion was crossed with a 1 keV electron beam from an electron gun and anions were formed via secondary-electron attachment to neutral molecules and clusters [12]. Water clusters were formed from residual water vapor trapped in the gas lines.

* Corresponding author. Fax: +1 520 621 8407.
E-mail address: sanov@u.arizona.edu (A. Sanov).

[1] National Science Foundation Research Experience for Undergraduates student, visiting the University of Arizona from Sonoma State University, Rohnert Park, CA, USA.

0009-2614/$ - see front matter © 2012 Elsevier B.V. All rights reserved.
http://dx.doi.org/10.1016/j.cplett.2012.08.035

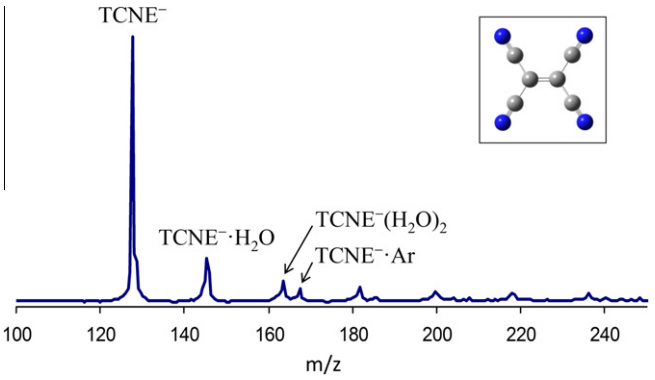

Figure 1. Representative time-of-flight mass spectrum. Inset shows the D_{2h} symmetry equilibrium structure of neutral TCNE. The geometry of the anion is similar. See Refs. [4,5] for calculated structural parameters.

The anions are extracted into a Wiley-McLaren time-of-flight spectrometer, where they are separated by the mass-to-charge ratio and detected with a microchannel plate (MCP) detector mounted at the far end of the flight tube. In the detection region of the instrument, the ion beam is intersected with a linearly polarized pulsed laser beam, synchronized in time with the ion of interest. The third (355 nm, 4 mJ/pulse) or fourth (266 nm, 2 mJ/pulse) harmonics of a Nd:YAG (Yttrium Aluminum garnet) laser (Quanta Ray, Lab 50, 8 ns pulse duration) was used in this work. Two types of experiments were performed: photoelectron imaging and photofragment mass-spectrometry.

Photoelectron images are recorded using a perpendicular (with respect to the ion beam) velocity-map [13] photoelectron imaging [14,15] assembly [11]. The photodetached electrons are projected onto a 40 mm diameter position sensitive MCP detector (Burle, Inc.) by means of the electric field defined by a series of velocity-map imaging electrodes. Raw images are recorded using a 1 megapixel charged-coupled device (CCD) camera and accumulated for $\sim 10^6$ experimental cycles. The reconstruction of the cylindrically symmetric (with respect to the laser polarization direction) three-dimensional probability distribution from the images is performed via inverse Abel transform [15] using the BASEX program [16]. The known photodetachment transition of O^- [17,18] was used to calibrate the electron kinetic energy (eKE) scale of the images. Photoelectron spectra were fit to sums of Gaussian functions using a standard algorithm for accurate determination of solvation energies. The corresponding photoelectron angular distributions were not analyzed in this work.

The photofragment-ion mass-spectra were recorded using a single-stage linear-field reflectron [11]. The fragment masses were determined by scanning the reflectron retardation potential while monitoring the ion signal with an off-axis MCP detector, as described previously [19]. Typically, 512 time-traces are averaged for each ion fragment. Stitching the averaged traces together yields the final photofragmentation spectra presented here.

3. Results and discussion

A representative time-of-flight mass spectrum corresponding to the parent ions of interest is shown in Figure 1. The photoelectron images of the bare $TCNE^-$ anion and the $TCNE^-\cdot Ar$ cluster obtained at 355 nm are presented in Figure 2. The corresponding spectra, plotted versus electron binding energy, $eBE \equiv h\nu - eKE$, are shown alongside the images (blue lines). The photoelectron images and spectra of $TCNE^-$, $TCNE^-\cdot Ar$ and $TCNE^-\cdot H_2O$ collected at 266 nm are shown in Figure 3. All images exhibit notable noise and distortions, attributed to the low signal levels. On this account, no attempt was made to analyze the photoelectron angular distributions. The low-pass filter Fourier analysis, described previously [20], was performed on all data sets presented and the resulting 'clean' photoelectron spectra, intended to guide the eye, are plotted in gray together with the raw data in Figures 2 and 3.

The 355 nm $TCNE^-$ and $TCNE^-\cdot Ar$ photoelectron images in Figure 2 reveal perceptible rings. In the corresponding spectra, the lower-eBE transitions are labeled collectively as band X. This band consists of at least four overlapping sub-bands, marked with ticks in the figure. These sub-bands are assigned to electron detachment from the ground state of the anion to the lowest vibrational levels (marked as 0–3) of the ground electronic state of the neutral. The vibrational interval is estimated at $\sim 500\ cm^{-1}$. From the position and width of the first peak in the 355 nm $TCNE^-$ spectrum, the adiabatic electron affinity of TCNE is determined as EA = 3.16 ± 0.02 eV. This is the first spectroscopic determination of this crucial property of TCNE. The result is in excellent agreement with the previous indirect determination of EA = 3.17 ± 0.20 eV [10], but reflects an order-of-magnitude smaller uncertainty range.

The low-eKE (i.e., high-eBE) bands in the photoelectron spectra, labeled with lower case a and b in Figure 2, are assigned to autodetachment from either $TCNE^-$ or one of the fragments produced in the photodissociation of the anion. The autodetachment peaks are less intense in the $TCNE^-\cdot Ar$ spectrum, consistent with the expectation that an Ar tagged cluster should be vibrationally cold, resulting in colder fragments.

The lowest-eBE bands in the 266 nm photoelectron spectra of $TCNE^-$, $TCNE^-\cdot Ar$ and $TCNE^-\cdot H_2O$ (Figure 3) correspond to the same ground-state anion to ground-state neutral transition as in Figure 2, so they are also labeled X. Due to the lower resolution for the higher kinetic energy electrons in 266 nm photodetachment, the low-frequency vibrational progression within the X band, partially resolved in Figure 2, is not observed in Figure 3. However, a higher-frequency progression with a $\sim 2100\ cm^{-1}$ interval is apparent in the 266 nm spectra. This progression is not observed in Figure 2, because its second band ($eBE \approx 3.5$ eV) is either greatly suppressed in the 355 nm spectra due to the threshold proximity or indistinguishable from the low-eKE autodetachment bands (a–b). We cautiously assign this progression to the CN stretch in neutral TCNE [21] Similar to 355 nm, the spectra in Figure 3 exhibit sharp low-eKE peaks that do not shift as a result of solvation. These peaks are assigned to autodetachment of excited $TCNE^-$ or vibrationally excited photofragments.

The $TCNE^-\cdot H_2O$ spectrum in Figure 3 is shifted towards higher binding energy by about 0.35 eV. This shift defines the hydration energy that can be calculated from the thermodynamic cycle: $D_0(A^-\cdot X) = EA(A\cdot X) + D_0(A\cdot X) - EA(A)$. It is often assumed that solvent binding energy to the anion is much greater than that to the corresponding neutral, i.e. $D_0(A^-\cdot X) \gg D_0(A\cdot X)$, in which case $D_0(A^-\cdot X) \approx EA(A\cdot X) - EA(A)$. If so, the above spectral shift of 0.35 eV corresponds to a hydration energy that is quite small compared to that of many smaller anions. For reference, the first hydration energy of O_2^- is 0.967 eV [22], while that of I^- is 0.46 eV [23]. It is possible that the hydration energy of neutral TCNE is not negligible and, if accounted for, will increase the above estimate for the anion hydration. However, the low first hydration energy of $TCNE^-$ is consistent with the delocalized-charge structure of $TCNE^-$ [4,5] and its asymmetric solvation, whereas the water molecule is expected to be bonded to only one or at most two of the four electronegative CN groups, interacting effectively with only a fraction of the excess charge [24]. This interpretation finds further support in that no discernible solvation-induced shift is observed in the $TCNE^-\cdot Ar$ photoelectron spectra at either 355 or 266 nm. A typical Ar binding energy to a small anion is ~0.05 eV [25], which is greater than the resolution and uncertainty limit in Figure 2. We expect that the Ar solvation energy may also be decreased significantly

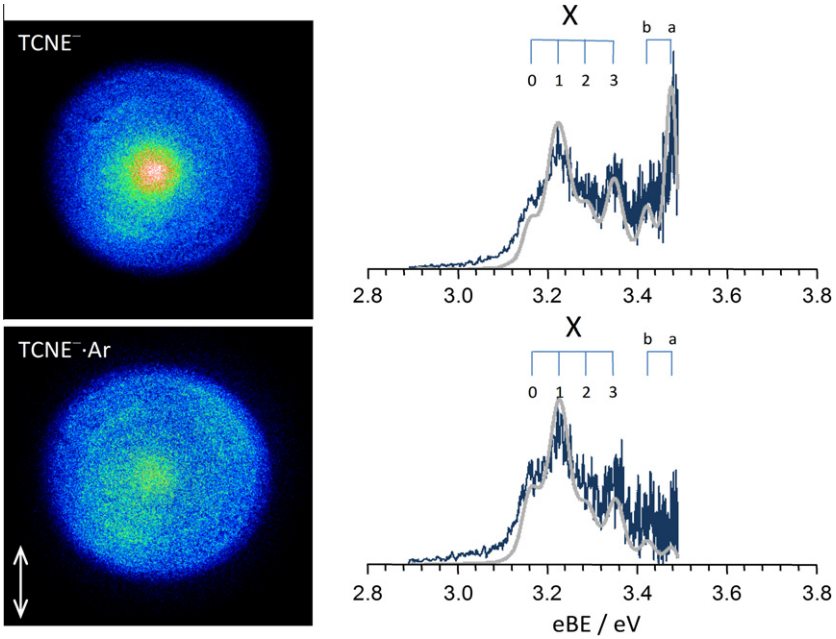

Figure 2. Photoelectron images and corresponding photoelectron spectra of $TCNE^-$ and $TCNE^-$·Ar cluster obtained at 355 nm. Vertical double arrow indicates the laser polarization direction. The experimental spectra are shown in blue. The gray curves are the result of a low-pass filter Fourier analysis. See the text for explanation of the spectral band assignments. (For interpretation of the references to color in this figure legend, the reader is referred to the web version of this article.)

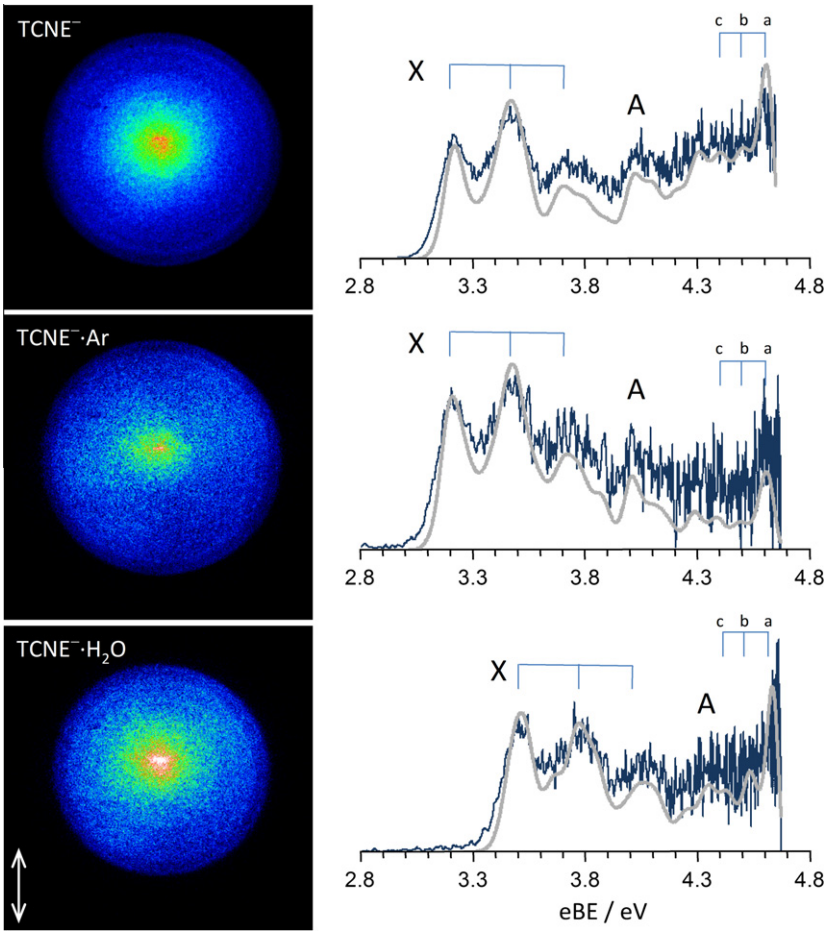

Figure 3. Photoelectron images of $TCNE^-$, $TCNE^-$·Ar and $TCNE^-$·H_2O collected at 266 nm. Vertical double arrow indicates the laser polarization direction. The experimental spectra are shown in blue. The gray curves are the result of a low-pass filter Fourier analysis. See the text for explanation of the spectral band assignments. (For interpretation of the references to color in this figure legend, the reader is referred to the web version of this article.)

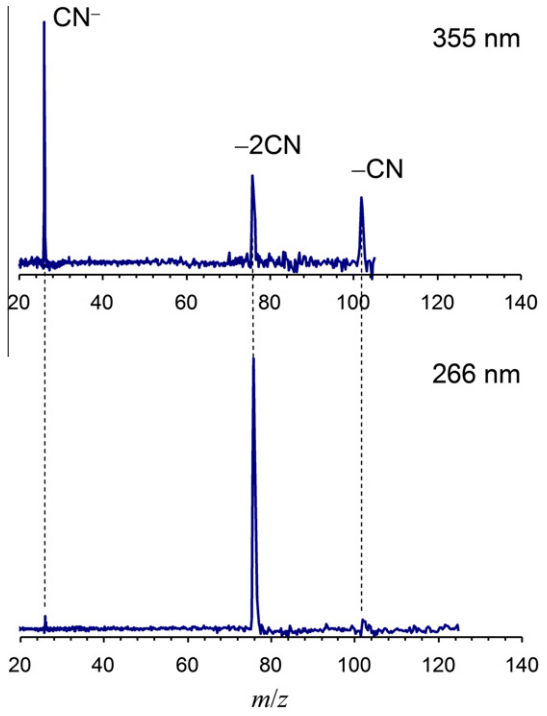

Figure 4. Photofragment-ion mass-spectra for $TCNE^-$ obtained at 355 and 266 nm. −CN and −2CN indicate the $m = 102$ and 76 a.m.u. fragment anions, i.e., $C_2(CN)_3^-$ and $C_2(CN)_2^-$, corresponding to the loss of one or two CN groups from parent $TCNE^-$, respectively.

relative to the small-anion value, due to the large size and delocalized charge distribution of $TCNE^-$.

Figure 4 displays the photofragment-ion mass-spectra for $TCNE^-$ obtained at 355 and 266 nm. Three types of fragment ions are observed in different proportions at both wavelengths: CN^- ($m = 26$ a.m.u.) and the $m = 102$ and 76 a.m.u. ions corresponding to the loss of one or two CN groups from parent $TCNE^-$, respectively. The CN and 2CN loss fragments are indicated as –CN and –2CN, respectively in Figure 4. This fragmentation pattern is consistent with the accepted structure of $TCNE^-$ (see the inset in Figure 1). The CN^- channel dominates the fragmentation at 355 nm, but the double dissociation (–2CN) fraction increases drastically at 266 nm compared to 355 nm, which may be accounted for by the greater available energy.

4. Summary

We reported the first spectroscopic determination of the adiabatic electron affinity of TCNE in the gas phase, EA = 3.16 ± 0.02 eV. This result represents an order-of-magnitude improvement in precision compared to the previous indirect determination [10]. Three anionic photofragmentation channels are observed for $TCNE^-$ at 355 and 266 nm: one yielding the CN^- fragment and the other two corresponding to the loss of one or two CN groups from the parent anion. The CN^- channel dominates the fragmentation at 355 nm, while the double-dissociation (−2CN) channel dominates the radical anion photochemistry at 266 nm.

Acknowledgements

This Letter was supported by the U.S. National Science Foundation (Grant CHE-1011895). D.K. acknowledges partial support from the State of Arizona TRIF Imaging Fellowship program. M.T.F. would like to thank the National Science Foundation for support through the Research Experience for Undergraduates program at the University of Arizona in the summer of 2011.

References

[1] J.S. Miller, Inorg. Chem. 39 (2000) 4392.
[2] M.L. Kaplan, R.C. Haddon, F.B. Bramwell, F. Wudl, J.H. Marshall, D.O. Cowan, S. Gronowitz, J. Phys. Chem. 84 (1980) 427.
[3] A.J. Fatiadi, Synth. Stuttg. (1987) 959.
[4] B. Milian, R. Pou-Amerigo, R. Viruela, E. Orti, Chem. Phys. Lett. 375 (2003) 376.
[5] B. Milian, R. Pou-Amerigo, M. Merchan, E. Orti, ChemPhysChem 6 (2005) 503.
[6] A.J. Fatiadi, Synth. Stuttg. (1986) 249.
[7] S.J. Blundell, Appl. Magn. Reson. 13 (1997) 155.
[8] J.R. Fox, B.M. Foxman, D. Guarrera, J.S. Miller, J.C. Calabrese, A.H. Reis, J. Mater. Chem. 6 (1996) 1627.
[9] S. Fukuzumi, K. Mochida, J.K. Kochi, J. Am. Chem. Soc. 101 (1979) 5961.
[10] S. Chowdhury, P. Kebarle, J. Am. Chem. Soc. 108 (1986) 5453.
[11] L. Velarde, T. Habteyes, A. Sanov, J. Chem. Phys. 125 (2006) 114303.
[12] M.A. Johnson, W.C. Lineberger, in: J.M. Farrar, W.H. Saunders (Eds.), Techniques for the Study of Ion Molecule Reactions, Wiley, New York, 1988, pp. 591–635.
[13] A.T.J.B. Eppink, D.H. Parker, Rev. Sci. Instrum. 68 (1997) 3477.
[14] D.W. Chandler, P.L. Houston, J. Chem. Phys. 87 (1987) 1445.
[15] A.J.R. Heck, D.W. Chandler, Annu. Rev. Phys. Chem. 46 (1995) 335.
[16] V. Dribinski, A. Ossadtchi, V.A. Mandelshtam, H. Reisler, Rev. Sci. Instrum. 73 (2002) 2634.
[17] D.M. Neumark, K.R. Lykke, T. Andersen, W.C. Lineberger, Phys. Rev. A 32 (1985) 1890.
[18] S.J. Cavanagh, S.T. Gibson, M.N. Gale, C.J. Dedman, E.H. Roberts, B.R. Lewis, Phys. Rev. A 76 (2007) 052708.
[19] D.J. Goebbert, A. Sanov, J. Chem. Phys. 131 (2009) 104308.
[20] D.J. Goebbert, D. Khuseynov, A. Sanov, J. Phys. Chem. A 115 (2011) 3208.
[21] J.S. Miller, Angew. Chem. Int. Ed. 45 (2006) 2508.
[22] A.K. Luong, T.G. Clements, M.S. Resat, R.E. Continetti, J. Chem. Phys. 114 (2001) 3449.
[23] R. Mabbs, E. Surber, A. Sanov, J. Chem. Phys. 122 (2005) 054308.
[24] W.H. Robertson, E. Price, J.M. Weber, J.-W. Shin, G.M. Weddle, M.A. Johnson, J. Phys. Chem. A 107 (2003) 6527.
[25] J.H. Hendricks et al., J. Chem. Phys. 116 (2002) 7926.